Pergamon

Acta mater. Vol. 46, No. 2, pp. 579–584, 1998

Printed in Great Britain
PII: S1359-6454(97)00242-5
1359-6454/98 $19.00 + 0.00

FRACTURE PROPERTIES OF GaAs–AlAs SUPERLATTICES STUDIED BY ATOMIC FORCE MICROSCOPY AND SCANNING ELECTRON MICROSCOPY

M. R. CASTELL†, A. HOWIE and D. A. RITCHIE
Cavendish Laboratory, Madingley Road, Cambridge, CB3 0HE, U.K.

(Received 3 July 1997; accepted 10 July 1997)

Abstract—GaAs–AlAs superlattices with periodicities of up to 200 nm were cleaved to expose (110) faces. These surfaces were studied using high resolution scanning electron microscopy where the secondary electron images reveal contrast between the GaAs and AlAs layers and also indicate that the AlAs layers are topographically raised with respect to the GaAs. Atomic force microscopy of the same samples shows that the AlAs ridges can extend as far as 55 nm beyond the GaAs surface. Further secondary electron images of cross-sections of plastically deformed GaAs–AlAs superlattices reveal that the AlAs layers can undergo severe deformation whereas the GaAs layers fracture more readily. It is proposed that the AlAs protrusions on the (110) cleavage surface are due to the fracture behaviour of the superlattice as well as oxidation effects. © *1998 Acta Metallurgica Inc.*

1. INTRODUCTION

The unique electronic and optical properties of low dimensional structures has resulted in extensive studies of their microstructure. Quantum confinement effects can be correlated with the quality of the interfaces and uniformity of the layers as determined by transmission electron microscopy, sputter assisted evaluation, or optical methods. Surface sensitive microscopy such as atomic force microscopy (AFM) is also extensively used, but this relies on the creation of a flat cross-section through the quantum well region. This can be readily achieved on most III–V semiconductors as they cleave with relative ease on (110) planes. Previous reports on scanning probe microscopy studies of (110) cross-sections through GaAs–AlGaAs [1–4] and GaInAs–InP [5–7] superlattices have revealed that, even without chemical etching, corrugations with the superlattice periodicity are seen. The corrugation height is generally of the order of less than a nanometre and has been attributed to either differences in the electronic properties of the quantum wells affecting scanning tunnelling microscope (STM) imaging [5, 6] or preferential oxidation of one of the phases giving rise to topograpical differences [1, 3, 4, 6].

The only mention that the corrugations might be due to the cleavage process itself was rejected by Kato *et al.* [5] on the grounds that both cleavage surfaces were mirror images of each other, which is also in agreement with the observations presented in this paper. Kato *et al.* state that a cleavage artefact should result in the two opposite faces being inverses of each other. In their view, the experimental observation of the mirror image faces is inconsistent with a cleavage artefact. However, here we show that during cleavage of GaAs–AlAs superlattices the GaAs layers fracture readily whereas the AlAs layers deform plastically before fracture, resulting in AlAs protrusions on both cleavage surfaces with heights of up to 55 nm.

2. EXPERIMENTAL PROCEDURE

The GaAs–AlAs superlattices used in the experiments were grown in a VG Semicon V80H molecular beam epitaxy (MBE) system on (001) GaAs substrates. Cross-sectional cleavage exposing a (110) surface was peformed in air and within half an hour the samples were introduced into the vacuum chamber of a Hitachi S900 scanning electron microscope (SEM). The immersion lens geometry and field emission gun of this microscope make sub-nanometre resolution possible in secondary electron (SE) imaging mode. The SE images presented in this paper were all taken using primary electrons with energies of 20 keV or 25 keV. The topography of cleavage surfaces of samples (prepared in the same way as for the SEM experiments) was investigated in ambient conditions with a Nanoscope II AFM using microfabricated Si tips.

†To whom all correspondence should be addressed. Present address: Department of Materials, University of Oxford, Parks Road, Oxford OX1 3PH, U.K..

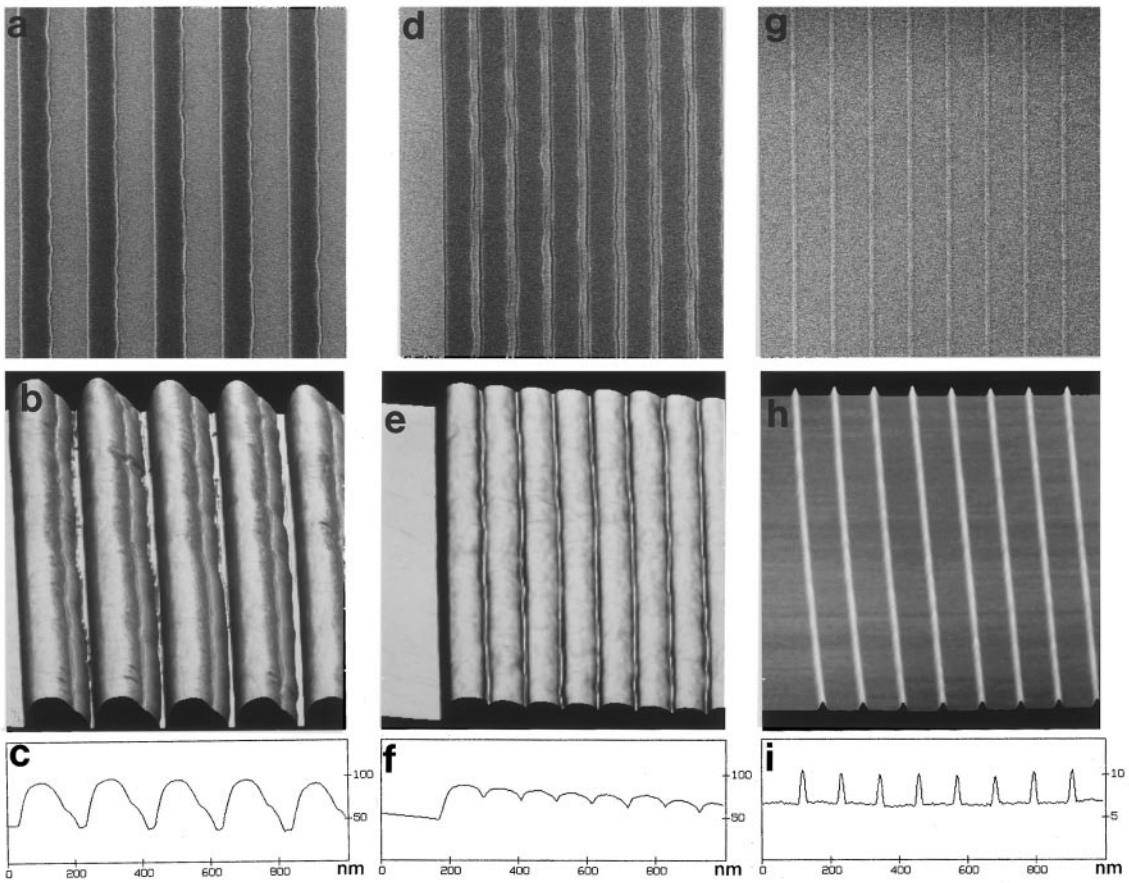

Fig. 1. Secondary electron (a,d,g) and atomic force microscope (b,e,h) images of (110) cleavage surfaces of GaAs–AlAs superlattices of differing layer thicknesses. In the SE images (a,d) taken at 20 keV, the GaAs and AlAs layers appear bright and dark, respectively, and are separated by dark–light doublets. In the SE image in (g) the AlAs layers appear bright owing to their topography. The surface imaged by AFM shows that the AlAs layers have formed ridges of 55 nm, 45 nm, and 4 nm heights in images b, e, and h, respectively. Typical AFM linescans perpendicular to the layers are shown in parts c, f, and i. All image widths are 1 μm.

3. RESULTS AND DISCUSSION

Figure 1 shows corresponding AFM and SEM images, as well as AFM linetraces, of the (110) cleavage surface of three GaAs–AlAs superlattices. The SEM images were taken at 20 keV in the SE imaging mode. The SE contrast across the layers in Fig. 1(a) can be explained as follows. The light grey regions are GaAs, and the dark layers are AlAs, which is due to the greater SE emission coefficient of GaAs compared with AlAs [8–10]. The layer widths measured from the micrograph are 90 nm and 109 nm for the AlAs and GaAs layers respectively. At the edges of the AlAs layers the image appears bright owing to the increased SE signal at abrupt changes in topography [11]. The bright ridge indicates the top of a step and is accompanied by a dark region next to it where SE emission at the bottom of the step is reduced. At the irregular (right hand) side of the AlAs layers, the dark region is highly pronounced which indicates the presence of a deep cavity, presumably caused by delamination of the layer. This delamination is only present on one side of the layers but can occur on both sides as shown in Fig. 1(d).

The sample topography of Fig. 1(a), as imaged by AFM, is shown in Fig. 1(b). It is immediately apparent that the image has been adversely affected by the shape of the probe tip. Where one would expect a trace of approximately the form of a square wave, the linetrace in Fig. 1(c) shows that during scanning the AFM tip only just reaches the bottom of the troughs between the AlAs ridges. Although the AFM data cannot be viewed as an accurate representation of the true surface topography, it contains reliable information on the periodicity of the superlattice and the height of the AlAs ridges. The periodicity was measured to be 200 nm $\pm$ 6 nm, which may be compared with 199 nm $\pm$ 8 nm determined from the SE micrograph in Fig. 1(a). The AlAs ridge heights were found to be

surprisingly large at 55 nm $\pm$ 3 nm, as can be seen in Fig. 1(c).

The lack of variation of the SE contrast across the GaAs layers at the bottom of the troughs indicates that the SE signal contributing to the image is highly localized. The contrast between the GaAs and AlAs layers must therefore be due mainly to two effects. Firstly, the differences in stopping power between the materials (GaAs has a higher stopping power than AlAs). This will give rise to greater SE emission at the beam entrance point in GaAs relative to AlAs. Secondly, the additional SEs that are created in the higher atomic number material (GaAs) when high angle elastically backscattered electrons exit the material [10].

Figure 1(d) shows an image of a GaAs–AlAs superlattice grown to different specifications from the one discussed above. The SE micrograph in Fig. 1(d) reveals that the dark AlAs layers are significantly thicker than the bright GaAs layers, and fine dark–bright doublets can be seen at the steps between the layers. In this micrograph delamination between the layers is more clearly pronounced than in Fig. 1(a). The superlattice periodicity measured from the SE micrograph is 108 nm $\pm$ 4 nm, compared with a value of 111 nm $\pm$ 3 nm determined by AFM [Fig. 1(e)]. As the troughs between the AlAs ridges are 26 nm $\pm$ 2 nm, i.e. narrower than in the sample shown on Fig. 1(b), the AFM tip only indicates the presence of the troughs and is not able to image their true depth. However, the AlAs ridge height of 45 nm $\pm$ 2 nm may be determined by measuring the height of the left most AlAs ridge, as seen in the linescan in Fig. 1(f).

The SE image of a GaAs–AlAs superlattice consisting mainly of GaAs is shown in Fig. 1(g). The sample was cleaved to expose the superlattice which consists of 8.6 nm $\pm$ 0.5 nm AlAs layers and 97.8 nm $\pm$ 3 nm GaAs layers, as determined using growth-rate data and X-ray diffraction. As was the case with the previous GaAs–AlAs superlattices, the AlAs layers formed ridges, but in this case the width of the layers is so small that the high SE yield at either side of the ridge causes the whole ridge to appear brighter than the GaAs. The AlAs ridges therefore appear bright owing to topographic contrast, which more than offsets the low SE yield from AlAs compared with GaAs. The superlattice periodicity, measured from the SE micrograph and AFM data [Fig. 1(h)] was 111 nm $\pm$ 3 nm and the AlAs ridge height was 4 nm $\pm$ 0.5 nm, as seen in the AFM linescan in Fig. 1(i).

Figure 2 is an SE micrograph of the (110) cleavage face of a GaAs–AlAs superlattice with approximately 155 nm periodicity. Distinct steps can be seen on the surface, and at each step the AlAs layers protrude beyond the GaAs. Severe deformation and cracking can be achieved through indentation of these samples. Figure 3 is a (110) cleavage cross-section through a 2 N Vickers microindentation. This micrograph shows quite clearly that the AlAs layers can undergo severe plastic deformation prior to fracture. Almost every crack contains bridging AlAs layers which appear highly ductile in comparison with the GaAs. The indenta-

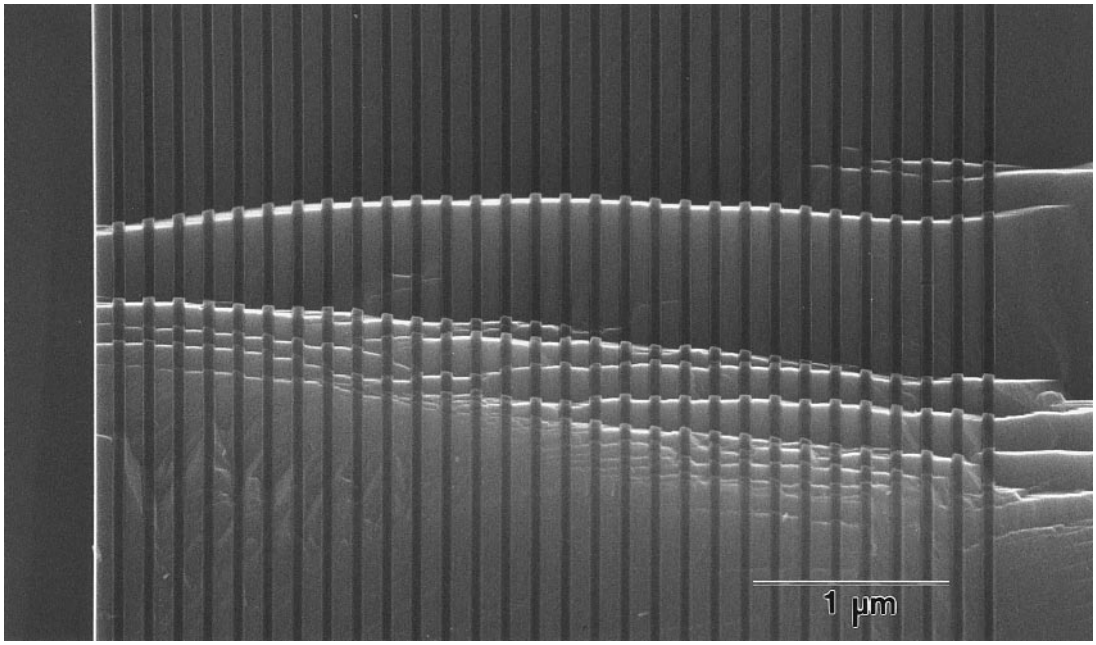

Fig. 2. Secondary electron micrograph, taken at 25 keV, of steps on the cleavage surface of a GaAs–AlAs superlattice. The steps appear as bright jagged lines running horizontally across the image. The AlAs layers (dark) protrude beyond the GaAs (light) at the step edges.

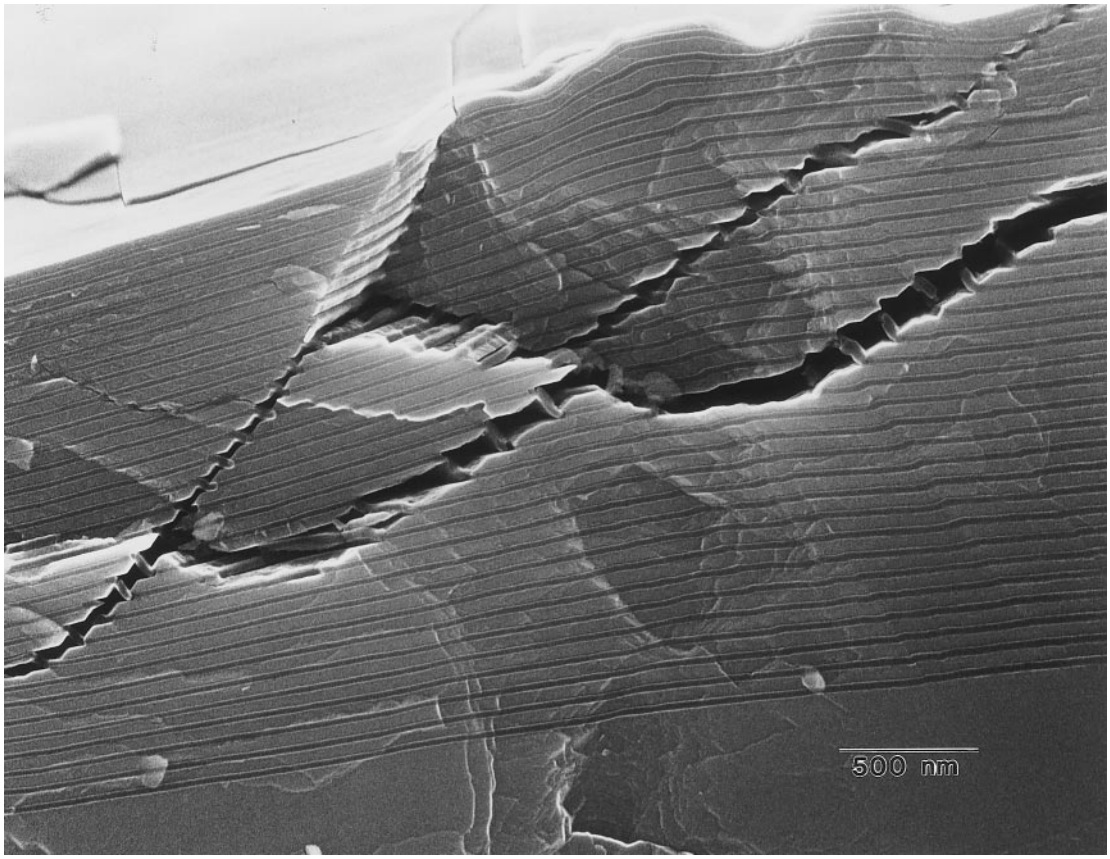

Fig. 3. Extensive fracture of a GaAs–AlAs superlattice caused by Vickers indentation. The secondary electron micrograph, taken at 20 keV, shows bridging of the AlAs layers (dark) across cracks in the GaAs (light).

tion response of GaAs–AlAs superlattices has previously been discussed in Ref. [12].

The AlAs ridges are seen on both cleavage surfaces, so an effect like fibre pull-out in a fibre composite material is not occurring. It seems most likely that sample cleavage results in the AlAs layers being plastically deformed before fracturing, whereas the GaAs layers seem to cleave without undergoing plasticity. This results in the creation of AlAs ridges on both sides of the exposed cleavage surfaces, as shown schematically in Fig. 4. The probable sequence of events of the cleavage crack running through the GaAs–AlAs superlattice is as follows. When the crack reaches an AlAs layer it will not immediately be able to propagate into it as the stress field at the crack tip will not be great enough to cause fracture. This is because the fracture toughness is larger for AlAs than GaAs. As the layer interfaces are relatively weak, cracks will run perpendicular to the cleavage crack, resulting in debonding at the interfaces. Initially the AlAs layer will experience tensile elastic deformation and the crack will re-nucleate in the GaAs on the far side of the AlAs layer. This situation is shown schematically in Fig. 4. By now the AlAs layer has started to deform plastically and continues to do so until crack nucleation occurs and causes the layer to fracture. How many AlAs layers are being deformed at a given time during cleavage will vary. In Fig. 4 there is only one AlAs layer that is undergoing plasticity prior to fracture, but the number depends on materials properties such as layer thicknesses and crack velocity in the GaAs. The type of fracture that appears to be occurring in the GaAs–AlAs superlattices is similar to that observed in ductile-dispersion toughened ceramics where the ceramic matrix is toughened by the inclusion of ductile metal particles [13].

One of the most important materials properties in the analysis of fracture behaviour is the plane strain fracture toughness, K_{Ic}, which is a measure of the resistance to crack propagation in a material. Generally, brittle ceramics have a value of $K_{Ic} < 3$ MPa $m^{1/2}$. For GaAs $K_{Ic} = 0.44$ MPa $m^{1/2}$, and for AlAs, $K_{Ic} = 1.7$ MPa $m^{1/2}$ [14]. Although K_{Ic} of AlAs is almost four times greater than that of GaAs the value is still in the region where one would expect brittle fracture to occur in the bulk materials. However, values of K_{Ic} are size dependent and it is usually observed that K_{Ic} increases as the dimensions of the sample decrease. In the case of nanometre sized layers of GaAs and AlAs the

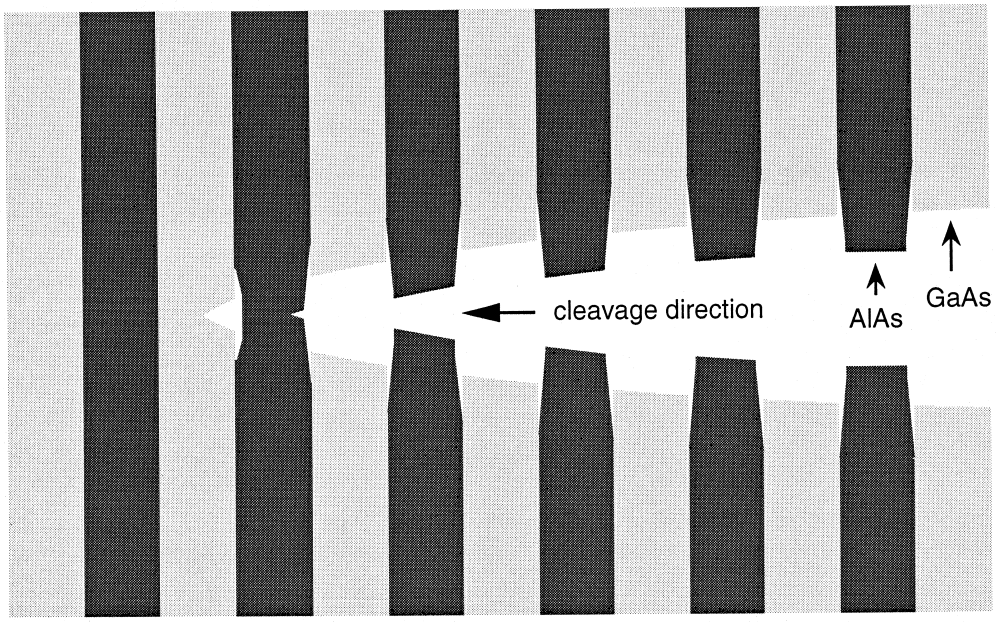

Fig. 4. Schematic illustration of the cleavage of a GaAs–AlAs superlattice. As the crack propagates the AlAs layers are plastically deformed prior to fracture resulting in a series of AlAs ridges on both cleavage faces.

values of K_{Ic} are certain to be much greater than for the bulk materials. As can be seen in the schematic diagram of the fracture process (Fig. 4), the layered nature of the material and the interfaces between the layers both play an important role. The type of cleavage mechanism discussed above is entirely different from the situation in a bulk sample of GaAs or AlAs. As the crack propagates through the superlattice there are continuous crack re-nucleation events as well as plastic deformation of the AlAs layers. This means that the fracture toughness of one of these types of superlattice should be significantly greater than the average of its components. Size dependent effects are commonly observed in fracture mechanics and could explain why AlAs in a layered form behaves differently from the bulk material.

4. CONCLUSION

We have shown that cleavage of GaAs–AlAs superlattices results in the creation of AlAs ridges formed by plastic deformation of the AlAs layers during fracture. Previous observations of small corrugations (less than a nanometre) observed on cleaved AlGaAs–GaAs superlattices were most likely correctly attributed to preferential AlGaAs oxide formation, but the results on GaAs–AlAs superlattices presented here show that larger corrugation amplitudes are mainly due to AlAs layer plasticity. We have carried out similar experiments to those described above on a variable composition GaAs-superlattice and have not observed this unusual fracture behaviour. As can be seen in the SE images, the ridges have an almost rectangular cross-section and can be as high as 55 nm. If the ridges were oxide, one would expect them to have grown in a far more diffuse shape than the images suggest, and it is unlikely that the ridges could have attained a height of 55 nm. Conclusive evidence of AlAs plasticity is provided by the images of the deformed superlattices which show plastically elongated AlAs layers bridging cracks in the GaAs matrix.

It is possible that the type of GaAs–AlAs superlattices described in this paper could be incorporated into GaAs-based electronic devices that are prone to fracture. The ductile behaviour of the AlAs layers increases the fracture toughness of the material and causes reduced crack propagation perpendicular to the layers.

Acknowledgements—We are grateful to Dr D.A. Williams of the Hitachi Cambridge Laboratory who rendered valuable assistance in the SEM operation which was generously donated to the Cavendish Laboratory by Hitachi Ltd. We would also like to thank the EPSRC for funding the Cambridge MBE programme and the CASE studentship for MRC who was also supported by the National Physical Laboratory.

REFERENCES

1. Prohaska, T., Friedbacher, G., Grasserbauer, M., Nickel, H., Lösch, R. and Schlapp, W., *Anal. Chem.*, 1995, **67**, 1530.
2. Gwo, S., Chao, K-J. and Shih, C. K., *Appl. Phys. Lett.*, 1994, **64**, 493.
3. Friedbacher, G., Hansma, P. K., Schwarzbach, D., Grasserbauer, M. and Nickel, H., *Anal. Chem.*, 1992, **64**, 1760.

4. Chalmers, S. A., Gossard, A. C., Weisenhorn, A. L., Gould, S. A. C., Drake, B. and Hansma, P. K., *Appl. Phys. Lett*., 1989, **55**, 2491.
5. Kato, T., Osaka, F. and Tanaka, I., *Jap. J. Appl. Phys*., 1989, **28**, 1050.
6. Howells, S., Gallagher, M. J., Chen, T., Pax, P. and Sarid, D., *Appl. Phys. Lett*., 1992, **61**, 801.
7. Tamayo, J. and Garcia, R., *Mater. Sci. Engng*, 1996, **B42**, 122.
8. Bleloch, A. L., Castell, M. R., Howie, A. and Walsh, C. A., *Ultramicroscopy*, 1994, **54**, 107.
9. Perovic, D. D., Castell, M. R., Howie, A., Lavoie, C., Tiedje, T. and Cole, J. S. W., *Ultramicroscopy*, 1995, **58**, 104.
10. Merli, P. G., Migliori, A., Nacucchi, M., Govoni, D. Mattei, G., *Ultramicroscopy*, 1995, **60**, 229.
11. Reimer L., Scanning Electron Microscopy. Springer Series in Optical Sciences, Springer Verlag, Berlin, Vol. 45.
12. Castell, M. R., Howie, A., Perovic, D. D., Ritchie, D. A., Churchill, A. C. and Jones, G. A. C., *Phil. Mag. Lett*., 1993, **67**, 89.
13. Lawn B., Fracture of Brittle Solids—Second Edition. Cambridge University Press, Cambridge, 1993.
14. Hjort, K., Söderkvist, J. and Schweitz, J.-Å., *J. Mircomech. Microengng*, 1994, **4**, 1.